Phase and amplitude scintillations associated with polar cap patches: Statistical and event analyses

Alanah Cardenas-O'Toole[1], Shasha Zou[1], Jiaen Ren[1], Zihan Wang[1], and Jayachandran Thayyil[2]

[1]University of Michigan, Department of Climate and Space Sciences and Engineering [2]University of New Brunswick, Physics Department

CEDAR 2023: IRRI-9

1) Introduction

- Ionospheric scintillation can degrade the GNSS signals and has the potential to cause a loss of access to GNSS services.
- Figure 1 shows a visual representation of the impacts of ionospheric structures on communication and navigation, including polar cap patches.
- Using a polar cap patch database provided by Ren et al. [2018] and scintillation data from 2016 provided by CHAIN, we study whether and how polar cap patches impact ionospheric scintillation.
- **It was found that ~92% patches do not lead to significant phase or amplitude scintillation increases in the polar cap, but occasionally they do lead to enhanced scintillations and preferentially near noon.**

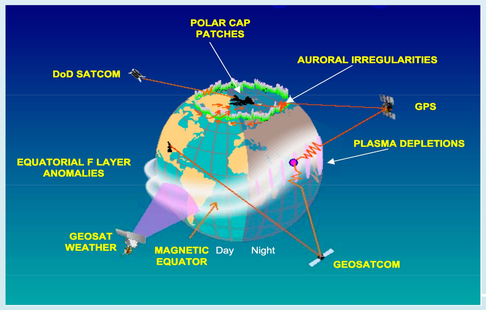

Figure 1. Schematic plot highlighting the ionospheric structures that can disrupt communication and navigation signals (image credit: UiO).

2) About the Data

- This study adapts a patch identifying algorithm from Ren et al. [2018] and applies it to the RISR-C data in 2016. Density enhancements in the F-region of the ionosphere that had a density at least double the surrounding plasma [Crowley, 1996] and had halfwidths that lasted between 3 minutes and 2 hours are defined as patches.
- We found 541 patches in 2016 and used 433 patches for this study with simultaneous scintillation measurements.
- The Canadian High Arctic Ionospheric Network (CHAIN) GPS receiver collocated with RISR-C provided the phase and amplitude scintillation data for the patches.
- In order to exclude multi-path effects and identify scintillation close to the RISR-C field-aligned beam, the ionospheric pierce points (IPPs) that corresponded to an elevation angle higher than 20 degrees were used.
- Other complementary data from AMPERE, SuperDARN, and solar wind monitor are also used to assist the interpretation of the scintillation events that were investigated.

3) Statistical Analysis

Patch Scintillation Distribution

- Figure 2 displays the distributions of amplitude (a) and phase (b) scintillations during the peak of polar cap patches.
- **Most of the amplitude scintillations fall below 0.3 (~ 92 %)**. 35 of the 433 events (~8%) displayed max amplitude scintillation above 0.3.
- **Most of phase scintillations also fall below 0.3 (~ 92%)**. 32 of the 433 events (~8%) displayed max phase scintillation above 0.3.
- Less than 1% of patches (3 of the 433 patches) displayed severe phase scintillation over 0.5. and none displayed severe amplitude scintillation.
- The patch edges showed similar distributions.

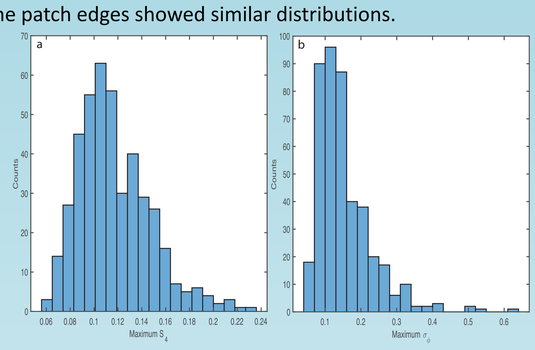

Figure 2. Histograms of the distribution of amplitude (a) and phase (b) scintillations during the peak of a polar cap patch.

MLT Dependence

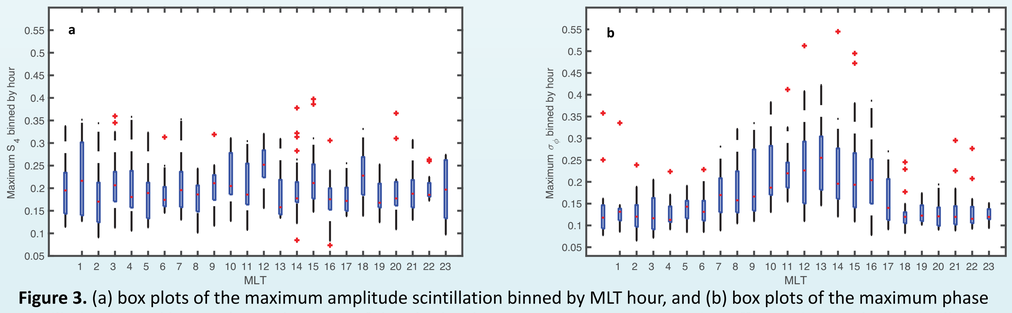

Figure 3. (a) box plots of the maximum amplitude scintillation binned by MLT hour, and (b) box plots of the maximum phase scintillation binned by MLT hour. The y axis of the plot has been cut to 0.05 to 0.55 cutting off a maximum phase scintillation value that is an outlier at y = 0.67 at 2 MLT.

- Figure 3 displays the MLT dependence of the scintillation values for the patch maximum at the density peak.
- The maximum amplitude (a) and phase (b) scintillation values during the patch are binned by MLT hour.
- It can be noted that there is an increase in the median of the phase scintillation (b) values near noon MLT.
- The relationship is not apparent in the amplitude scintillation as shown in (a).
- **These plots demonstrate that patches near noon, generally have higher phase scintillation.**

Patch Temperature Dependence

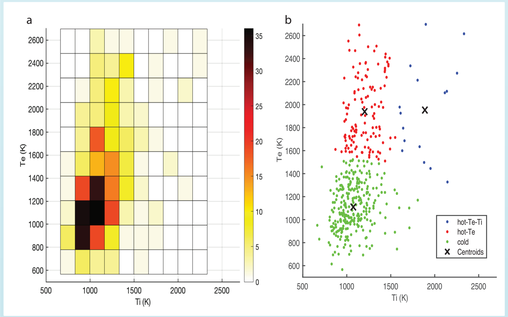

Figure 4. a) Mosaic plot of the ion and electron temperatures associated with polar cap patches (b) classifications of the patches by ion and electron temperatures divided into three categories: hot-Te (red) , hot-Te-Ti (blue), and cold (green)

- Figure 4 (a) shows the distribution of Te and Ti associated with patch in a 2D mosaic plot. The patch temperatures were calculated using a moving mean of 3 minutes.
- One can see that most the patches are below 1500 K for both Te and Ti, which would belong to the classical cold patch class
- To define a hot or cold patch, we used k-means clustering, a classification algorithm provided by MATLAB called kmeans, which finds k centroids for n data points. We chose k = 3, and the algorithm used the squared Euclidean distance to find the optimum clusters by measuring the distance between the different centroids and the data points.
- **Figure 4 (b) shows three different patch temperature classifications, including cold (Ti ~=Te <~1500 K), hot-Te (Te >> Ti and Te >~1500 K), and hot-Te-Ti (Ti~=Te >~1500 K).**

- Figure 5 shows the temperature dependence of the amplitude (a,b,c) and phase scintillation (d,e,f). The ion (a,d) and electron (b,e) temperatures are shown as well as the electron to ion temperature ratio (c,f). The magenta line is a linear fit of the scatter plots shown.
- Based on the correlation coefficients in the top right corner, it can be seen that the best fits are the Phase vs Te and Phase vs Te/Ti.
- This indicates that **the phase scintillation has a larger dependence on electron temperature and the temperature ratio than the amplitude scintillation does**.
- The larger correlations in Figure 5 (b) and (e) also show that the electron temperature has a higher correlation with the scintillation values for a polar cap patch than the ion temperature.

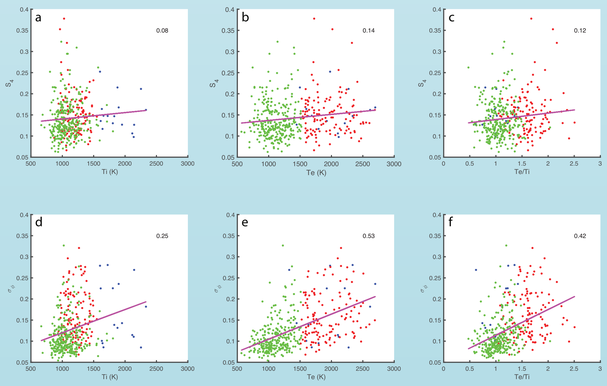

Figure 5. The amplitude (a,b, c) and the phase (d, e, f) as a function of Ti (a,d), Te (b,e), and Te/Ti (c,f) are shown. The magenta line is the linear fit, and the number in the top right corner is the correlation coefficient between the fit and the scatter plots. The points are color-coded by patch temperature as shown in Figure 4.

Temperature, Density, and MLT

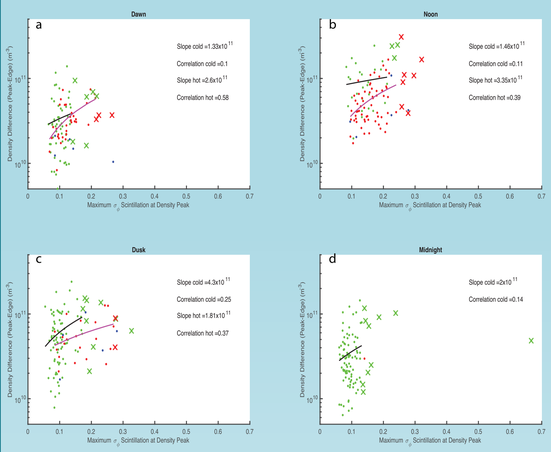

Figure 6. The density difference (peak - edge) as a function of maximum phase scintillation at the peak density for different MLT time periods. The black line is a linear fit of the cold patches, and the magenta line is a linear fit of the hot-Te patches.

- Figure 6 (phase) shows the distribution of hot-Te (red), cold (green), and hot-Te-Ti (blue) patches for different MLT sectors as labeled. The y axis is the density prominence of the patches, i.e., the difference between the peak and edge densities. The x axis is the peak maximum phase scintillation.
- The black lines show the linear fit the cold patches within the sector, while the magenta line shows the linear fit of just the hot-Te patches.
- For phase scintillation (Figure 5), the correlations that fall into the 95% confidence interval when excluding the patches outside of the 90th percentile are dusk cold patches, dawn hot-Te patches, and noon hot-Te patches.
- **This indicates that the phase scintillation of hot-Te patches during noon and dawn and cold patches during dusk are linearly related to the density prominence.**
- No correlations for the amplitude scintillation (not shown) fell into the the 95% confidence interval when excluding the patches outside of 90th percentile.

4) Event Analysis

- Figure 7 shows an example of hot-Te patch associated with enhanced scintillations on March 06, 2016. The patch occurred at 21:18 UT and is marked by a red circle.
- Looking at the density of the 21:18 UT patch, it can be noted that there are several density spikes in the span of this patch. This patch occurred at 14:18 MLT, which falls in the range of noon MLT.
- Figure 7 (b) and (c) show the phase and amplitude scintillations
- **During the patch, both the phase and amplitude scintillations are enhanced and there is a maximum phase scintillation value over 0.5 detected by PRN 9 just before the patch density peak.**
- **Although there is no significant amplitude scintillation detected, there is still an increase to >0.25, compared to the background scintillation detected at the peak of the patch by PRN 7 and PRN 29.**

Figure 7. Patch Density (a) with the peak marked by a red circle and a black line to mark the half width. Phase (b) and amplitude (c) scintillations between 20:00 UT and 22:00 UT on March 6, 2016. The black vertical line indicates a polar cap patch peak identified. The green vertical line represents the beginning of the patch, and the red vertical line identifies the end of the patch.

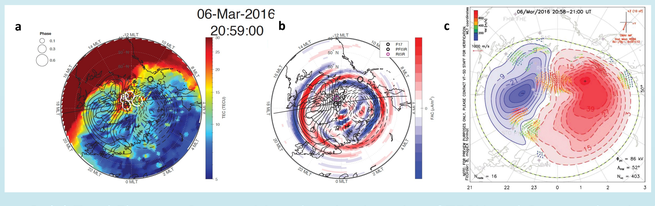

Figure 8. (a) Total Electron Content Map showing in units of TECU and Current density (b) on March 6, 2016 at 20:59 UT. (f) Ionosphere convection map for March 6, 2016 between 20:58 and 21:00 UT.

- Figure 8 show March 6, 2016 at 20:59 UT showing the TEC (a), the FACs (b), and the convection map (c) during the scintillation increase.
- RISR-C is shown by a magenta circle in (a) and (b) and was just poleward of the cusp, which can be found roughly between the large red and blue FAC density signatures at ~72 degrees around noon and the convection throat in Figure 8 (b).
- During this time period, the TEC increased on the dayside due to the storm-enhanced density (SED) and the plume extended poleward into the polar cap, which was then segmented into a patch.
- At 20:59 UT, the structured patch passed over RISR and the receivers causing an influx of severe phase scintillation as shown by the enlarged white circles.
- Figure 8 (c) shows the SuperDARN convection pattern with velocity vectors. The fast convection flows were detected right over the receiver suggesting field-aligned density irregularities just poleward of the cusp at this time, consistent with the TEC and RISR observations shown earlier.
- According to Zou et al. (2021), the storm that occurred on March 6, 2016 was caused by a CIR, which reached a minimum DST at 21:20 UT. This storm caused SED and polar cap patches during the ionospheric positive storm phase. In this study, it is noted that a polar cap patch was observed just poleward of the dayside cusp at ~21:18 UT on March 06, 2016 just before the minimum Dst of the storm, and enhanced phase scintillations were observed near the western edge of the patch and later to the east as the patch propagating across the receiver. These observations support the role of patch in creating enhanced ionospheric phase scintillation

5) Conclusion

1. It was found that 92% of the maximum patch scintillation was under 0.3 for both phase (in the unit of radian) and amplitude scintillations, and 8% of the maximum patch phase and amplitude scintillations exceeded 0.3. Less than 1% of the phase scintillation was classified as severe, i.e. over 0.5 radians, while no severe amplitude scintillation was identified associated with the patches in the database. The patch edges are not statistically different from the patch peaks in terms of scintillation values.
2. There is a clear MLT dependence of the patch phase scintillation with higher scintillation values near noon MLTs, while no such dependence is observed for amplitude scintillation.
3. The dependence of scintillation on the patch prominence has been evaluated at different sectors and a clear positive correlation can be found for cold patches near noon for max amplitude scintillation and for hot-Te patches everywhere except midnight for max phase scintillation. The phase scintillation is found to be more dependent on the patch density prominence than the amplitude scintillation.

For further questions, please contact alanahco@umich.edu

Acknowledgements

AC was supported by funding provided by Michigan Space Grant Consortium (MSGC), NASA FINESST 80NSSC22K1847 and NASA 80NSSC20K1313. SZ, JR and ZW are supported by NASA 80NSSC20K1313. AC would also like to thank Leslie Lamarche for helpful discussions and suggestions. The scintillation data at Resolute Bay were provided by CHAIN. The solar wind data were provided by NASA OMNIWeb service. The ionospheric FAC data were provided by AMPERE. The convection maps data were provided by SuperDARN. The VISTA TEC data were based on the Madrigal TEC data. The RISR data were provided by the University of Calgary and the Madrigal database.

References

Ren, J., Zou, S., Gillies, R. G., Donovan, E., & Varney, R. H. (2018). Statistical characteristics of polar cap patches observed by RISR-C. *Journal of Geophysical Research: Space Physics*, 123, 6981– 6995. https://doi.org/10.1029/2018JA025621

Zou S, Ren J, Wang Z, Sun H and Chen Y (2021) Impact of Storm-Enhanced Density (SED) on Ion Upflow Fluxes During Geomagnetic Storm. *Front. Astron. Space Sci.* 8:746429. https://doi.org/10.3389/fspas.2021.746429

Tore André Bekkeng,, "Prototype Development of a Multi-Needle Langmuir Probe System," Master Thesis, University of Oslo, Department of Physics, May 25, 2009, URL: http://www.duo.uio.no/publ/fysikk/2009/92317/bekkeng.pdf